Han *et al. Cell Regeneration* (2022) 11:23
https://doi.org/10.1186/s13619-022-00123-w

Cell Regeneration CSCB

RESEARCH ARTICLE Open Access

Interferon-beta inhibits human glioma stem cell growth by modulating immune response and cell cycle related signaling pathways

Xin-Xin Han[1*†], Shengkai Jin[2†], Li-Ming Yu[1], Min Wang[3], Xin-Yu Hu[4], Dai-Yu Hu[4], Jie Ren[4], Meng-Han Zhang[1], Wei Huang[1], Jia-Jia Deng[1], Qing-Qing Chen[1], Zhengliang Gao[4], Hua He[5,6*] and Chunhui Cai[4*]

Abstract

Malignant Glioma is characterized by strong self-renewal potential and immature differentiation potential. The main reason is that malignant glioma holds key cluster cells, glioma stem cells (GSCs). GSCs contribute to tumorigenesis, tumor progression, recurrence, and treatment resistance. Interferon-beta (IFN-β) is well known for its anti-proliferative efficacy in diverse cancers. IFN-β also displayed potent antitumor effects in malignant glioma. IFN-β affect both GSCs and Neural stem cells (NSCs) in the treatment of gliomas. However, the functional comparison, similar or different effects of IFN-β on GSCs and NSCs are rarely reported. Here, we studied the similarities and differences of the responses to IFN-β between human GSCs and normal NSCs. We found that IFN-β preferentially inhibited GSCs over NSCs. The cell body and nucleus size of GSCs increased after IFN-β treatment, and the genomic analysis revealed the enrichment of the upregulated immune response, cell adhesion genes and down regulated cell cycle, ribosome pathways. Several typical cyclin genes, including cyclin A2 (*CCNA2)*, cyclin B1 (*CCNB1)*, cyclin B2 (*CCNB2),* and cyclin D1 (*CCND1)*, were significantly downregulated in GSCs after IFN-β stimulation. We also found that continuous IFN-β stimulation after passage further enhanced the inhibitory effect. Our study revealed how genetic diversity resulted in differential effects in response to IFN-β treatment. These results may contribute to improve the applications of IFN-β in anti-cancer immunotherapy. In addition, these results may also help to design more effective pharmacological strategies to target cancer stem cells while protecting normal neural stem cells.

Keywords: Glioma stem cells, IFN-β, Neural stem cell, Cell cycle, Immune response

Background

Malignant glioma is highly aggressive and represents the most common primary brain tumors. The overall survival period is typically less than 15 months. Even with regular therapy, including surgical resection and chemoradiation, tumor recurrence appears to be inevitable (Ostrom et al. 2016). One year after diagnosis, approximately 70% of malignant glioma patients will facing the disease progression (Stupp et al. 2005). Thus, the use of personalized drugs that target molecular receptors and immunotherapy have been viewed as promising new options for glioma treatment (Davis 2016).

Malignant glioma is heterogeneous, with multiple epigenetic and genetic variations identified in associated

†Xin-Xin Han and Shengkai Jin contributed equally to this work.

*Correspondence: xxhan@fudan.edu.cn; hehua1624@smmu.edu.cn; pattycaich@tongji.edu.cn

[1] Shanghai Key Laboratory of Craniomaxillofacial Development and Diseases, Shanghai Stomatological Hospital & School of Stomatology, Fudan University, Shanghai, China
[4] Tongji University Cancer Center, Shanghai Tenth People's Hospital, School of Medicine, Tongji University, Shanghai, China
[6] Department of Neurosurgery, Third Affiliated Hospital of Second Military Medical University, Shanghai, China
Full list of author information is available at the end of the article

tumor cells. The intrinsic, aggressive behavior of malignant glioma has also been shown to depend on the complex tumor microenvironment (TME). Malignant glioma and their TME consist of GSCs, mature neural cells (oligodendrocytes, astrocytes, microglia, and ependymal cells), and some immune cells etc. (Abels et al. 2019; Broekman et al. 2018).

The identification of cancer stem cells in malignant glioma are first reported in 2002 (Ignatova et al. 2002). Several groups isolate and characterize stem-like cancer cells in glioma (Galli et al. 2004; Hemmati et al. 2003; Ignatova et al. 2002), which lead to the realization that GSCs are resistant to chemotherapy and radiotherapy (Bao et al. 2006; Chen et al. 2012). Some groups try to find the genes which regulate GSCs maintenance and glioma progression (Herrmann et al. 2020; Hu et al. 2016; Huang et al. 2021; Kim et al. 2021; Taga and Tabu 2020; Venkatesh et al. 2015; Wang et al. 2021). Inspire of so many struggles, the prognosis of GBM has not enhanced in the past decade (Wang et al. 2021). At the same time, the underlying mechanisms of GSCs survival after treatment remain unclear.

Interferon (IFN) factors are pleiotropic cytokines, it can be categorized into 3 classes. Type I IFNs include approximately 20 members. Human IFNs induce the Janus kinase–signal transducer (JAK) and activator of transcription (−STAT) cascade by binding to the IFN-α/β receptors (IFNARs), IFNAR1 and IFNAR2 (Lohmann et al. 2020; Platanias 2005). IFN-β signaling had been proved to inhibit cell proliferation in many types of cancer cells (Borden et al. 2000; Mizuno and Yoshida 1998; Natsume et al. 1999; Natsume et al. 2000; Yagi et al. 1994). During malignant glioma treatment, at least two aspects of neural stem cells (NSCs) are related to GSCs. On the one hand, mutated NSCs are considered to be the initiation cells of glioma (Alcantara Llaguno et al. 2019; Tian et al. 2020; Wang et al. 2021). On the other hand, normal NSCs are considered to have the ability to move towards GSCs, and can be used as carriers for the treatment of gliomas (Kendall et al. 2008; Schmidt et al. 2005). The human F3 NSCs cell line has been used in multiple studies to perform NSC-based gene therapy, delivering both IFN-β and cytosine deaminase (CD)/5-fluorocytosine (5-FC) prodrugs to glioma cells (Dickson et al. 2007; Kim et al. 2006; Shimato et al. 2007). Although IFN-β has been generally employed as a clinical treatment, whole-transcriptome analyses examining the effects of IFN-β stimulation in GSCs and NSCs are still rare. A systematic understanding of the genetic variations that occur following IFN-β treatments can provide additional evidence for the optimization of IFN-β-associated gene therapy for malignant glioma treatment in clinical trials.

In the present study, we used various doses of IFN-β to separately treat human GSCs (hGSCs) and human NSCs (hNSCs). Both morphological and genetic alterations were carefully observed and analyzed. We found that IFN-β increased the cell and nuclear size of hGSCs. The number of sphere-like cells observed in hGSC populations was reduced, both during short-term treatments and under conditions of continuous stimulation. However, INF-β did not appear to have the same or similar effects on hNSCs. Genomic analysis was performed to identify genes with expression changes in hGSCs but not in hNSCs. Immune response and cell adhesion genes were upregulated by IFN-β treatment, whereas the expression levels of cell cycle and ribosome genes were strongly reduced, which was consistent with our observations of the changed cell morphology. We observed that IFN-β preferentially restrained hGSCs rather than hNSCs. A few cyclin genes, including *CCNA2*, *CCNB1/2* and *CCND1*, downregulated in hGSCs after IFN-β treatment. Our exploration may facilitate to design new and more effective pharmacological strategies for killing hGSCs while protecting hNSCs during glioma treatment.

Results

IFN-β inhibits the growth of hGSCs

To detect the functional role of IFN-β in hGSCs, we first used IFN-β, at concentrations of 0, 0.625, 1.25, 2.5, 5, and 11 ng/mL, to treat the hGSCs (Fig. 1a). hGSCs typically display two types of cell morphologies: sphere-like hGSCs and adherent hGSCs (Fig. 1b). We quantified the area sizes of the sphere-like hGSC and the coverage of adherent hGSCs to examine the effects

(See figure on next page.)

Fig. 1 The growth of hGCSs but not hNSCs is inhibited by IFN-β. **a** A schematic representation showing hGCSs treated with basic media containing 10 ng/mL fibroblast growth factor (FGF), and different concentrations of IFN-β: 0, 0.625, 1.25, 2.5, 5, and 11 ng/mL. **b** The sphere-like hGCSs were inhibited, and more adherent hGCSs were observed after the IFN-β treatment. **c** IFN-β treatment resulted in smaller single sphere-like cells than control cells, and the sizes of the cell spheres are concentration-dependent within a certain range of IFN-β concentrations. **d** Coverage rate of adherent hGCSs decreased significantly with 5 ng/mL and 11 ng/mL IFN-β treatments. **e** Schematic representations of hGCSs treated with high concentrations of IFN-β. **f** High-concentration IFN-β also inhibits hGCS growth. **g** The coverage rate of hGCSs decreased after treatment with 11 ng/mL, 33 ng/mL, and 100 ng/mL IFN-β. **h** Schematic representation of hNSCs treated with high-concentration IFN-β. **i** High-concentration IFN-β does not inhibit hNSC growth. **j** The coverage rate of hNSCs does not decrease following treatment with 11 ng/mL, 33 ng/mL, and 100 ng/mL IFN-β. Quantitative data measured using ImageJ. Data are presented as the mean ± SD. Student's t-test. $*p < 0.05$, $**p < 0.01$, $***p < 0.001$

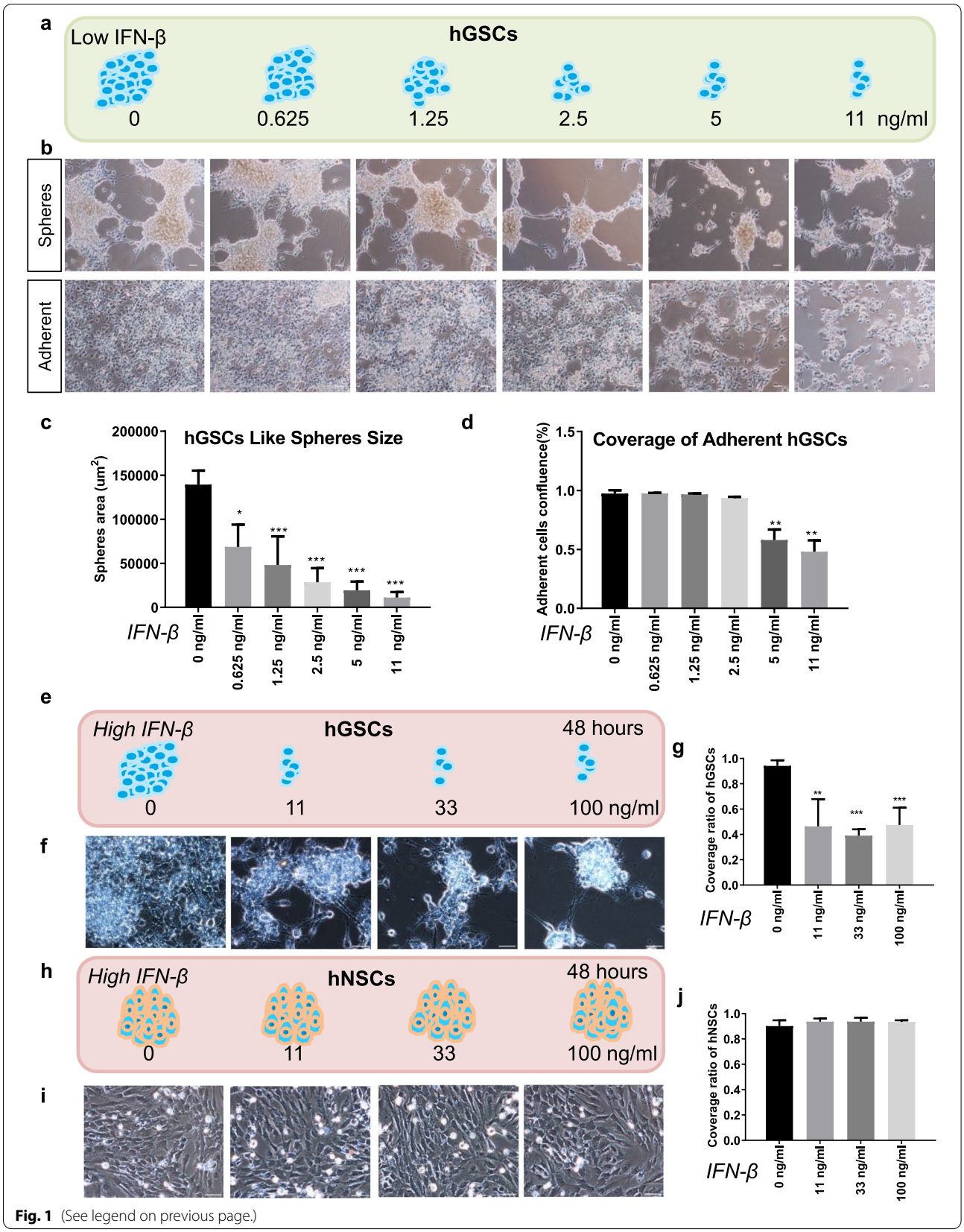

Fig. 1 (See legend on previous page.)

of IFN-β on cell growth. The sizes of the sphere-like hGSCs significantly decreased, even with the lowest treatment of 0.625 ng/mL IFN-β (Fig. 1c). However, no changes in the coverage of adherent hGSCs were observed until the treatment concentration reached 5 ng/mL IFN-β (Fig. 1d). These observations suggested that adherent hGSCs have a higher tolerance against IFN-β treatment than sphere-like cells. We repeated the treatment assay using higher IFN-β concentrations, including 11, 33, and 100 ng/mL, on both hGSCs and hNSCs (Fig. 1e, h). High dose of IFN-β also inhibited hGSC growth, but no significant morphological changes were observed with treated hNSCs (Fig. 1f, i). The quantitative analysis of cell coverage supported our visual observations (Fig. 1g, j). In conclusion, both low-dose (0.625 ng/mL) and high-dose (up to 33 ng/mL) IFN-β treatments were able to block cell growth in hGSCs, without affecting hNSCs.

The nuclear size of hGSCs was increased by IFN-β

We next performed immunostaining to detect the expression of Ki67, S100-β, and Sox2 in hGSCs after 6 days of treatment of IFN-β at both low (11 ng/mL) and high (33 ng/mL) doses. Similar to our morphological observations, the number of Ki67-positive hGSCs decreased after IFN-β treatment (Fig. 2a, b), as did the numbers of S100-β- and Sox2-positive cells (Fig. 2a, b). The quantitative assessment of Ki67, S100-β, Sox2, and DAPI nuclear stain in hGSCs following IFN-β stimulation can be seen in Fig. 2c. Because the total cell number decreased, the ratio of Ki67 to DAPI staining did not show a difference between the control group and the IFN-β-treated group. Overlapping images showed that the relative expression level of S100-β increased significantly after IFN-β stimulation (Fig. 3a). IFN-β might represent an effective agent for controlling cell differentiation in hGSCs (Yamamuro et al. 2015). S100-β has long been considered a biomarker for astrocytes (Castets et al. 1997). Recently, some studies have also identified the high expression levels of S100-β with malignant tumors (Imbalzano et al. 2020). The increased S100-β expression observed in hGSCs following IFN-β stimulation agrees with previous reports. The higher magnification image revealed the nuclear status (Fig. 3b). Representative images of DAPI staining and the schematic diagram of the nucleus revealed significant nuclear enlargement after IFN-β stimulation (Fig. 3c). The nucleus size was quantified using ImageJ, which revealed that the size of the nucleus increased in a dose-dependent manner following IFN-β treatment (Fig. 3d).

The cell growth and size of hGSCs was reduced by repetitive stimulation treatment with IFN-β

Clinically, IFN-β is administered over a long time course. Thus, we examined the effects of continuous IFN-β stimulation. Both hGSCs and hNSCs were cultured in either control medium or IFN-β medium for one generation (6 days), and then the control cells were passaged into control medium, whereas IFN-β-treated cells were separately passaged into both control medium and IFN-β medium (Fig. 4a), generating three groups of cells: control to control, IFN-β to control, and IFN-β to IFN-β. On day 2, the number of sphere-like hGSCs in the IFN-β to IFN-β group decreased compared with the numbers observed in the control to control group (Fig. 4b). The hGSCs conditions in IFN-β to control group showed more sphere-like cells than IFN-β to IFN-β group but fewer than observed in the control to control group. Although no significant effects were observed among hNSCs following short-term IFN-β stimulation (Fig. 1i), continuous IFN-β stimulation resulted in decreased cell growth (Fig. 4c). We observed these groups of cells again on day 8, which revealed very few surviving sphere-like cells in hGSCs within the IFN-β to IFN-β group (Fig. 4d). The enlargement of both the cell body and the nuclear size was also observed in this group (Fig. 4e). The hGSCs in the IFN-β to IFN-β group displayed an oligodendrocyte-like morphology, with a long and massive synapse (Fig. 4e). Quantitative analysis of hGSCs, including the coverage rate (Fig. 4f) and the single clone area (Fig. 4g), was performed on the surviving clones, which revealed significant reductions associated with IFN-β treatment.

Different gene responses in hGSCs and hNSCs after IFN-β treatment

To better understand the molecular mechanism associated with the IFN-β treatment effects observed in hGSCs and hNSCs, we performed RNA sequencing on samples treated with or without IFN-β in both hGSCs and hNSCs. Gene clustering analysis indicated the high quality of our

(See figure on next page.)

Fig. 2 IFN-β treatment resulted in decreased numbers of Ki67-, S100-β-, and Sox2-positive cells. **a** Representative images of hGCSs immunostained for Ki67, S100-β, and Sox2, with DAPI nuclear stain. Three groups, control, 11 ng/mL, and 33 ng/mL IFN-β treatment groups, were collected after 6 days of treatment (scale bar, 50 μm; white frames indicate the next part of the figure). **b** Representative images from (A), at higher magnification, using the same three groups: control, 11 ng/mL, and 33 ng/mL IFN-β treatment groups. **c** Quantitative analysis of Ki67, S100-β, Sox2, and DAPI nuclear stain in hGCSs after IFN-β stimulation, as measured by ImageJ. Data are presented as the mean ± SD. Student's t-test. $*p < 0.05$, $***p < 0.001$

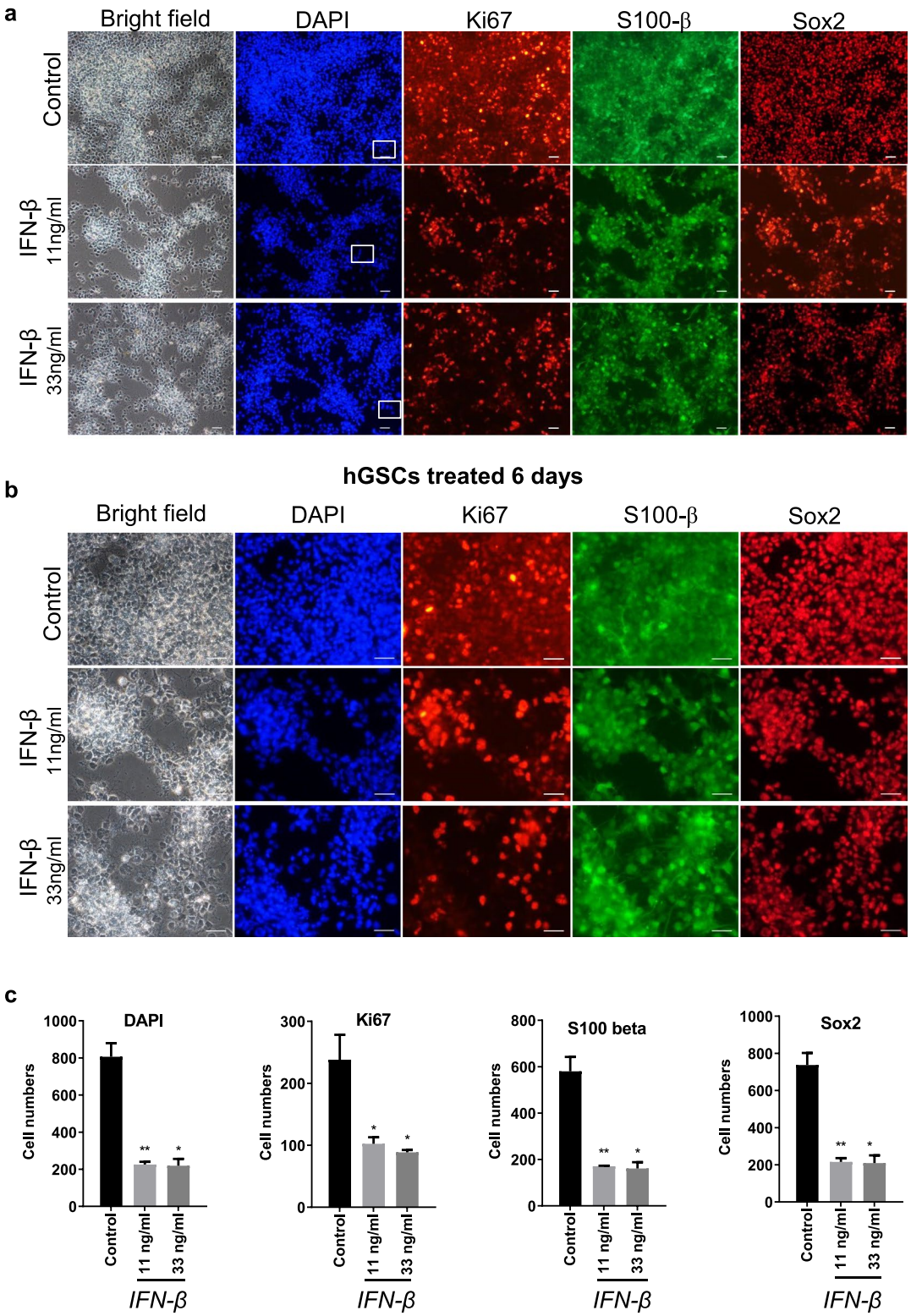

Fig. 2 (See legend on previous page.)

whole-transcriptome data (Fig. 5a). The analysis of different genes expression (DEGs) was used to identify genes that were up- and downregulated following IFN-β stimulation, resulting in 1707 and 1338 genes designated as $hGSC^{+}$ and $hGSC^{-}$ genes, respectively, whereas 1553 and 1169 genes were respectively designated as $hNSC^{+}$ and $hNSC^{-}$ genes (Fig. 5b). The integrative analysis of these four groups resulted in the identification of 995 genes characterized as $hGSC^{-}hNSC^{NA}$ (genes only downregulated in hGSCs but with no change in hNSCs) and 969 genes characterized as $hGSC^{+}hNSC^{NA}$ (genes only upregulated in hGSCs but with no change in hNSCs) (Fig. 5c). Then, we performed Kyoto Encyclopedia of Genes and Genomes (KEGG) and Gene ontology (GO) analyses on these two groups to further explore the potential downstream mechanisms associated with the response to IFN-β. The GO biological process (BP) analysis revealed that $hGSC^{+}hNSC^{NA}$ genes were primarily enriched in cytokine-mediated signaling, immune response, response to external stimulus, and cell adhesion pathways (Fig. 5d). The KEGG analysis revealed that $hGSC-hNSC^{NA}$ genes were enriched in the cell cycle and ribosome pathways (Fig. 5e). Our whole-transcriptome analysis results agreed with our previous morphological observations, supporting increased cell adherence and decreased cell growth. The expression patterns of the immune response and cell adhesion genes were displayed as heatmaps for both hGSCs and hNSCs (Fig. 5f). Consistent with known IFN-β downstream pathways, *JAK2*, *STAT6*, and *NFKB1*/2 were identified within the immune response pathways (Pfeffer et al. 2004; Platanias 2005; Yang et al. 2000). We also explored the detailed expression patterns of 22 genes in the cell cycle pathway (Fig. 5g). Typical cell cycle-related genes, such as *CCNA2*, *CCNB1*, *CCNB2,* and *CCND1,* were significantly downregulated following IFN-β stimulation in hGSCs but remained unchanged in hNSCs.

IFN-β decreased cell proliferation in hGSCs

IFN-β decreased hGSCs cell growth on both the morphological and genetic levels. Cell cycle-related genes were significantly downregulated after IFN-β stimulation (Figs. 5g and 6). The number of sphere-like cells also reduced significantly following IFN-β treatment, and both cell body and nuclear size increased. Simultaneously, genes associated with cell adhesion were upregulated in hGSCs, which supported the observed reductions in sphere-like cells and the enlargement of the cell nucleus. We also observed multiple synapses in hGSCs under conditions of continuous stimulation with IFN-β, and this morphological change may be associated with changes in gene expression in the immune response pathway.

Discussion

After stimulation of IFN-β, both the cell size and nuclear size of hGSCs increased. The increasement of nuclear size may directly correlated with the whole cell size enlargement. In both budding and fission yeasts, cells maintain a stable nuclear volume to cell volume ration at around 8% (Jorgensen et al. 2007; Neumann and Nurse 2007). Nuclear transfer experiment with Hela cells double confirmed that it is the cell size instead of DNA content to determine nuclear size (Cantwell and Nurse 2019). The cell size control mechanism is complex but important to maintain body homeostasis. The size theory suggested that cell division is based on a critical cell size (Cadart et al. 2018; Chien et al. 2012; Turner et al. 2012). In the yeast and bacteria studies, they indicated that large cells tend to proliferate faster than smaller ones (Chien et al. 2012; Turner et al. 2012). In mammalian cells, research of cell size distributions in populations of lymphoblasts shown support of the size theory. At the same time, researchers concluded that mammalian cells may have an intrinsic mechanism for cell size maintenance which is independent of cell cycle or age (Cadart et al. 2018; Son et al. 2012). In our data, the increased cell size did not correlate with faster cell growth. On the other side, less cell number and decreased cell cycle related gene expression have been observed after IFN-β stimulation in hGSCs. Similar phenomenon had been reported in mesenchymal stem cells (MSCs) before. MSCs had been separated as smaller and bigger cells (i.e., > 8-μm and < 8-μm) by pore transwell inserts, the sieved cells (< 8-μm) shown higher proliferative probability than un-sieved cells (> 8-μm) (Corradetti et al. 2011). In another study, the cellular thickness of MSCs had been measured with atomic force microscopy. Their results also suggested that small cells had high proliferative activity while large and flat cells have low proliferative activity (Katsube et al. 2008). The correlation between cancer stem cells (CSCs) and cell size had been investigated in prostate cancer cell lines PC3 by cell cytometry sorting technique (Li et al. 2015). The functional roles test shown

(See figure on next page.)

Fig. 3 Merged images showing the relative expression level of S100-β and the increased size of the cell nucleus after IFN-β stimulation. **a** Representative overlapping images showing staining for Ki67/DAPI, S100-β/DAPI, Sox2/DAPI, Ki67/S100-β, and Sox2/S100-β in hGCSs. Three groups, control, 11 ng/mL, and 33 ng/mL IFN-β treatment groups (yellow frames indicate enlarged areas). **b** Representative images from (a) at higher magnification. White arrows indicate S100-β expression. Enlarged area (scale bar, 50 μm). **c** Representative images of DAPI staining and a schematic diagram of the nucleus. **d** Quantitative analysis of nuclear size, as measured using ImageJ. Scale bar, 50 μm. Data are presented as the mean ± SD. Student's t-test. ***$p < 0.001$

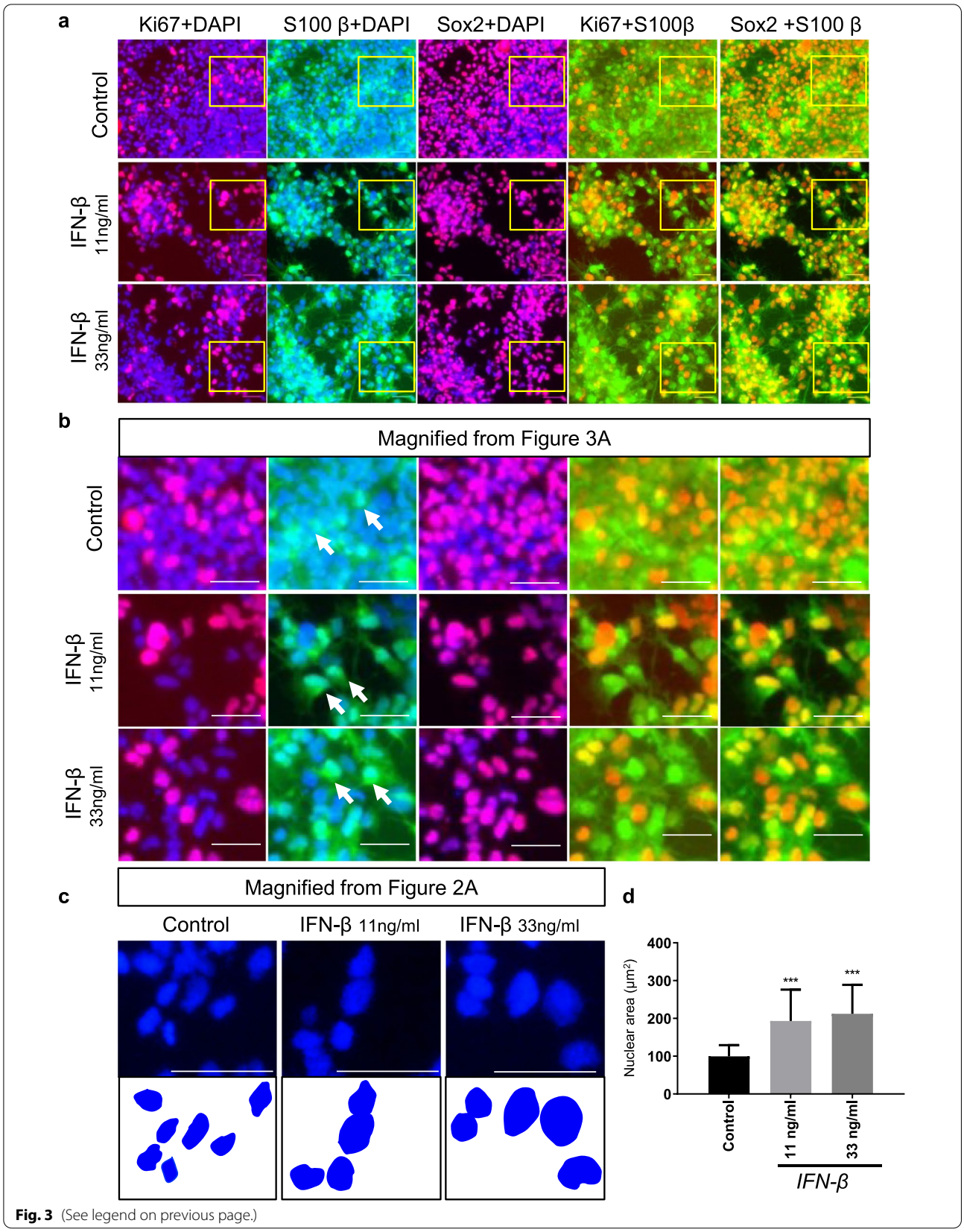

Fig. 3 (See legend on previous page.)

that large PC3 cells (≧ 20 or 30 μm) demonstrated lower clonal capacity and less tumorigenic ability than small PC3 cells (< 10 μm) (Li et al. 2015). However, it is still not clear which type of mechanisms coordinate cell growth and proliferation in metazoan cells (Li et al. 2015). Cell size enlargement and decreased cell proliferative ability in our study support the previous correlation of cancer stem cells and their sizes, further genomic analysis with different sizes of cancer stem cells may help us better understand the molecular mechanisms.

Our results indicated that IFN-β affected hGSCs rather than hNSCs. hNSCs are considered to be the most likely initiation cells of malignant glioma (Alcantara Llaguno et al. 2019; Tian et al. 2020; Wang et al. 2021). On the other hand, hNSCs have been considered efficient vehicles for the delivery of anti-cancer agents to tumor sites during therapeutic applications (Tang et al. 2017; Yamazoe et al. 2015). IFN-β has been found to exert antiproliferative effects in many cancer cell types (Ito et al. 2010; Sims et al. 2008). In glioma cell lines, IFN-β can inhibit cell cycle S-phase to decrease cell proliferation and progression (Garrison et al. 1996). However, the underlying molecular mechanisms responsible for the subsequent differences observed following IFN-β treatment between cancer stem cells and normal NSCs remain unclear. Microarray-based gene expression profiling performed in three glioma cell lines and primary B-cells following IFN-β treatment was reported in 2014 (Happold et al. 2014; Khsheibun et al. 2014). In primary B-cells, several novel IFN-β response genes were identified including *NEXN*, *HAPLN3*, *DDX60L,* and *IGFBP4* (Khsheibun et al. 2014). In this study, RNA sequencing was performed to reveal the molecular mechanisms associated with the response to IFN-β. We explored potential IFN-β response genes in glioma cells by performing DEG analysis between hGSCs and hNSCs. A total of 969 genes were identified as IFN-β-upregulated genes, whereas 995 genes were identified as IFN-β-downregulated genes in hGSCs compared with hNSCs. This large number of genes provides multiple opportunities to identify potential therapeutic targets that can be combined with IFN-β treatments for clinical applications.

A previous study indicated that IFN-β could induce spherogenicity in hGSCs (Happold et al. 2014). In our study, we noticed a significant reduction in sphere-like cells following IFN-β stimulation. The Gene Ontology (GO) analysis results indicated enrichment in cell adhesion genes, providing strong support for a functional role of IFN-β in cancer stem cell morphology. *NEXN* encodes nexilin, which acts as a linker protein for the cytoskeleton and affects focal adhesion junctions (Ohtsuka et al. 1998). *NEXN* was detected as a novel IFN-β response gene in multiple sclerosis (Khsheibun et al. 2014). In the whole-transcriptome analysis following IFN-β treatment, *NEXN* was identified as a top gene in the enriched cell adhesion pathway in hGSCs after IFN-β treatment. Therefore, *NEXN* may also represent a novel IFN-β response gene in hGSCs.

The genes that were downregulated by IFN-β treatment were primarily enriched in cell cycle pathways, which also provides evidence to support the previously identified inhibitory role of IFN-β in cancer cells (Garrison et al. 1996; Ito et al. 2010; Sims et al. 2008). A total of 22 cell cycle-related genes were found to be downregulated in hGSCs, but no significant differences were observed in hNSCs. We suggested that these 22 genes may play irreplaceable roles in response to IFN-β treatment in hGSCs. Recently, one study attempted to combine IFN-β treatment together with a novel, effective, cyclin-dependent kinase (CDK) inhibitor (TG02), which is used clinically to treat GBM (Le Rhun et al. 2019; Su et al. 2018; Wu et al. 2017), resulting in synergistic functions in human glioma models (Lohmann et al. 2020). In our data, *CDK1* was identified in the genomic analysis. Many other well-known cell cycle-related genes, such as the cyclin family genes (*CCNB1*, *CCND2*, *CCNB2,* and *CCNA2*), and MCM family genes (*MCM4*, *MCM5,* and *MCM6*), were also identified. These results may facilitate the development of more efficient therapeutic options by guiding the selection of useful anti-tumor drugs.

In our study, we included both hGSCs and hNSCs from previous studies (Han et al. 2017; Han et al. 2021). For each cell type, we include two cell lines for RNA sequencing analysis. Around 1500 genes regulated by IFN-β have been successfully identified with DGE analysis (Fold change > 2) as shown in Fig. 5b. Then we draw venn diagram to help us better understand the distribution of these genes. To better understand the specific roles of IFN-β on hGSCs rather

(See figure on next page.)

Fig. 4 Continuous IFN-β stimulation can enhance the inhibitory effects on hGCS growth, which differs from the effects on hNSCs. **a** Flow chart indicating the continuous stimulation timeline and imaging time points. The strategy of passage → stimulation → waiting → re-passage → stimulation → time point photography was adopted. **b** Representative hGCS images after continuous stimulation, re-passage, and stimulation, day 2. Three groups: control to control, IFN-β to control, and IFN-β to IFN-β (black frames indicate enlarged areas). **c** Representative hNSC pictures after continuous stimulation, re-passage, and stimulation, day 2. Three groups: control to control, IFN-β to control, and IFN-β to IFN-β (black frames indicate the enlarged area). **d** Representative hGCS images after continuous stimulation at re-passage, day 8. **e** Schematic diagram of hGCSs and hNSCs after re-passage and stimulation, day 2. **f**-**g** Quantitative analysis of hGCSs, including coverage rate (F) and single-clone area (G), of the surviving clones, as measured by ImageJ. Scale bar, 50 μm. Data are presented as the mean ± SD. Student's t-test. $**p < 0.01$, $***p < 0.001$

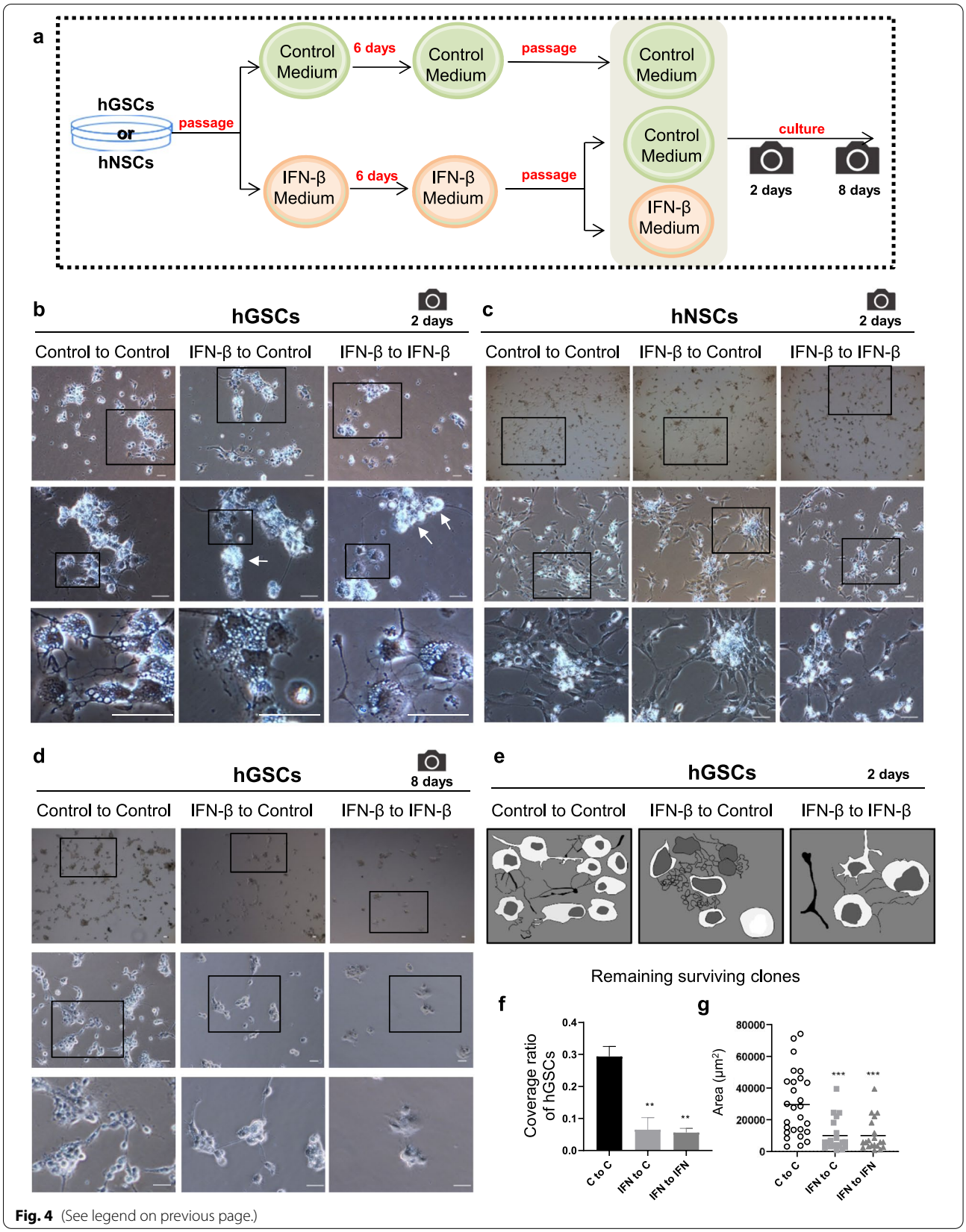

Fig. 4 (See legend on previous page.)

than hNSCs, we only focus on 969 genes upregulated in hGSCs ($hGSC^{+}hNSC^{NA}$) and 995 genes downregulated in hGSCs ($hGSC^{-}hNSC^{NA}$) as shown in Fig. 5c. Together with the morphological modification in hGSCs under IFN-β stimulation, we narrow down our target on cell cycle and cell adhesion pathways with KEGG and GO analysis. Further transcriptional analysis with multiple cell lines or primary tissues from these two different cell types may help us to deeply understand the underneath molecular mechanism. Also, the investigation of different dosages of IFN-β stimulation combined with regular chemotherapy drug, such as Temozolomide will be more persuasive for clinical consideration.

Conclusions

In summary, our study established the inhibition effects of IFN-β in hGSCs rather than in hNSCs. Additional morphological details were observed following IFN-β stimulation, such as larger cell bodies and nuclear sizes, fewer sphere-like cells, and more oligodendrocyte-like synapses. The subsequent transcriptional analysis using RNA sequencing was highly consistent with our morphological observations of hGSCs. The enrichment of genes involved in the cell cycle and cell adhesion pathways supported the observed reduction in cell growth and the morphological changes associated with IFN-β treatment. In addition, our exploration of the genetic modification that occurs after IFN-β treatment in both hGSCs and hNSCs may benefit the design of new and more effective pharmacological strategies for GBM treatment.

Methods

Cell culture

hGSCs line was established from surgical specimens (Han et al. 2021). Surgical specimens were gotten strictly according to Ethics Committee permission. Informed consents were introduced to glioma patients. All surgical specimens were donated with patients' permission. Tumor samples were delivered to the laboratory immediately after surgery for subsequently procedures. Briefly, after surgery, surgical specimens were collected for primary culture. The specimens were washed with 1× Hank's Balanced Salt Solution (HBSS, Gibco) at least six times. Then, the specimens were cut into small pieces, and the tissue fragments were transferred into 15 mL centrifuge tubes containing 1 U/mL Dispase II (Roche) in 3 mL Dulbecco's Modified Eagle Medium (DMEM)/F12 (Gibco) and kept in water-bath at 37 °C for 30 minutes to allow digestion. After digestion, the specimens were centrifuged at 1000×g for 3 minutes. The supernatant was discarded, and the tissues were resuspended with 3 mL DMEM/F12, followed by centrifugation. Finally, the precipitate was resuspended in growth medium (DMEM/F12 supplemented with N-2, B-27, GlutaMAX, bFGF, EGF, heparin and penicillin-streptomycin) for daily culture. All the work concentration of FGF, EGF and heparin were 20 ng/Ml, N-2, GlutaMax and penicillin-streptomycin were 100X while B-27 were 50X in the culture medium.

hNSCs line was generated from human embryonic stem cells (hESCs) (Han et al. 2017). Brief description, StemPro Accutase (Thermo Fisher) was used to digest the hESCs for 20 min at 37 °C. The cells were plated onto gelatin-coated plates for 1 hour at 37 °C. Because hESCs remain suspended, whereas mouse embryonic fibroblast (MEF) cells are adherent and separate hESCs from MEFs. The non-adherent hESCs were washed and seeded on Matrigel-precoated dishes in MEF-conditioned medium. Then we changed the medium to remove the ROCK inhibitor after 24 hours. Single adherent hESCs were expanded in cell medium until they were almost confluent. Noggin (500 ng/mL, R&D) and transforming growth factor-beta (TGF-β) inhibitor (10 mmol/L, Tocris) were added to confluent cells. The medium was replaced every 2 days with fresh KSR medium and different concentration gradients N2B27 medium. After nearly 10 days of differentiation, 100% N2 medium (DMEM/F12 supplemented with N2, GlutaMAX, EGF, FGF, heparin, penicillin, and streptomycin) was used to culture NSCs for one more day. Then, we transferred NSCs into a 100% N2/B27 medium (DMEM/F12 supplemented with N2, GlutaMAX, B27, FGF, EGF, heparin, penicillin and streptomycin).

Plate coating

NSCs induction plates were coated with gelatin (Sigma) or Matrigel (BD). Human NSCs culture plates were precoated with poly-L-ornithine (Sigma) and laminin (Thermo Fisher). The 24-well plates and 6-well plates were freshly coated with gelatin or Matrigel incubating overnight at 4 °C to improve packing effects. The next day, the dishes were treated with 0.5 μg/mL poly-L-ornithine (dissolved in water) at room temperature for 16 h. Then,

(See figure on next page.)

Fig. 5 Genomic changes in hGCSs after IFN-β treatment. **a** Gene clustering from control (Con-1 and Con-2) and IFN-β treatment (IFN-1 and IFN-2) samples for the hGCSs/hNSCs RNA sequencing results. **b** Identification of significantly upregulated and downregulated genes as $hGCS^{+}$ (1707 genes), $hGCS^{-}$ (1338 genes), $hNSC^{+}$ (1553 genes), and $hNSC^{-}$ (1169 genes). **c** The Venn diagram shows the overlap among the 4 gene lists identified in (B) to identify $hGCS—hNSC^{NA}$ (995 genes) and $hGCS^{+}hNSC^{NA}$ (969 genes) lists. **d** Biological process (BP) items in the Gene Ontology analysis of the $hGCS^{+}hNSC^{NA}$ gene list. **e** KEGG analysis of the $hGCS^{-}hNSC^{NA}$ gene list. **f** Expression patterns of immune response and cell adherent genes in hGCSs and hNSCs. **g** Expression patterns of cell cycle genes in hGCSs and hNSCs

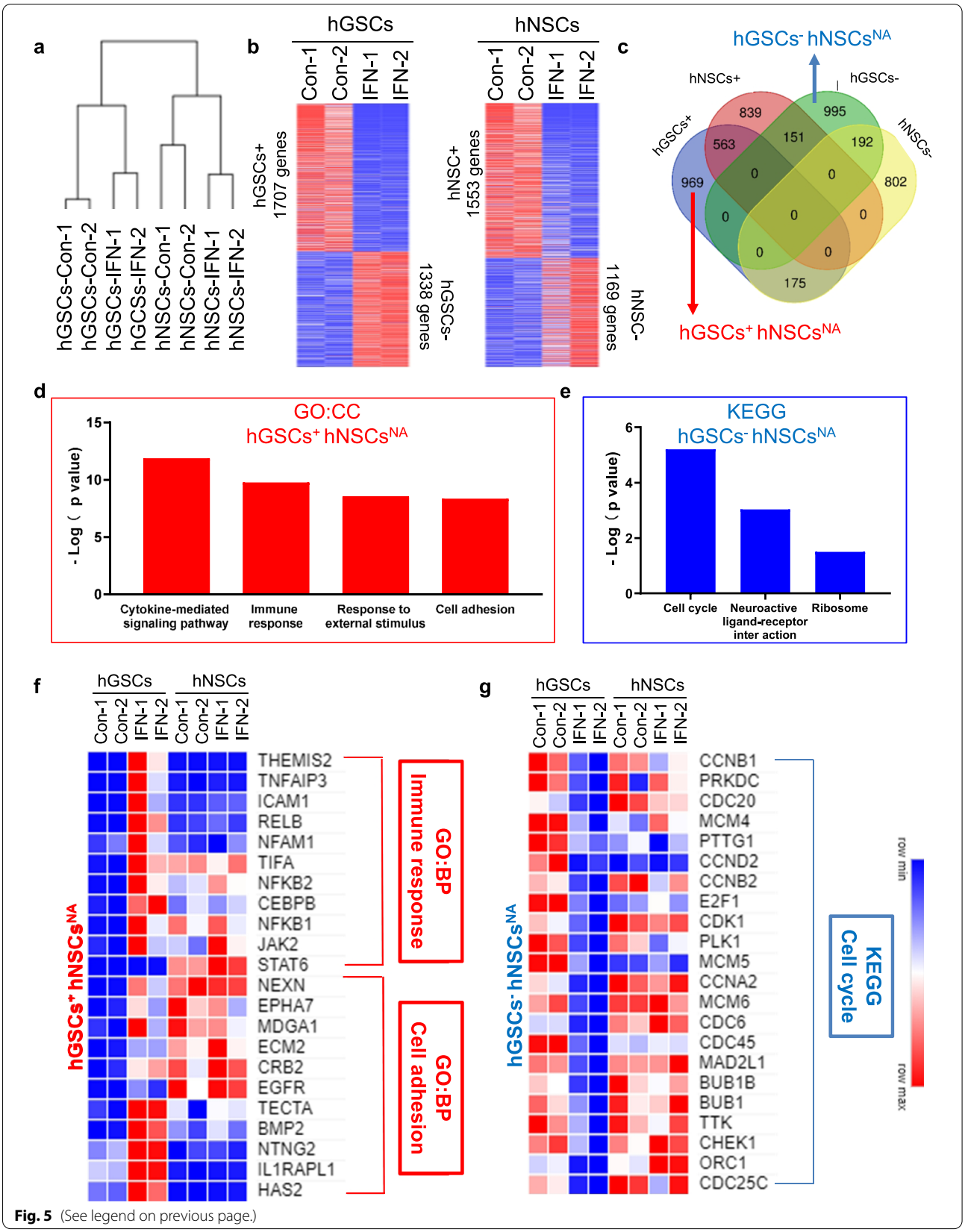

Fig. 5 (See legend on previous page.)

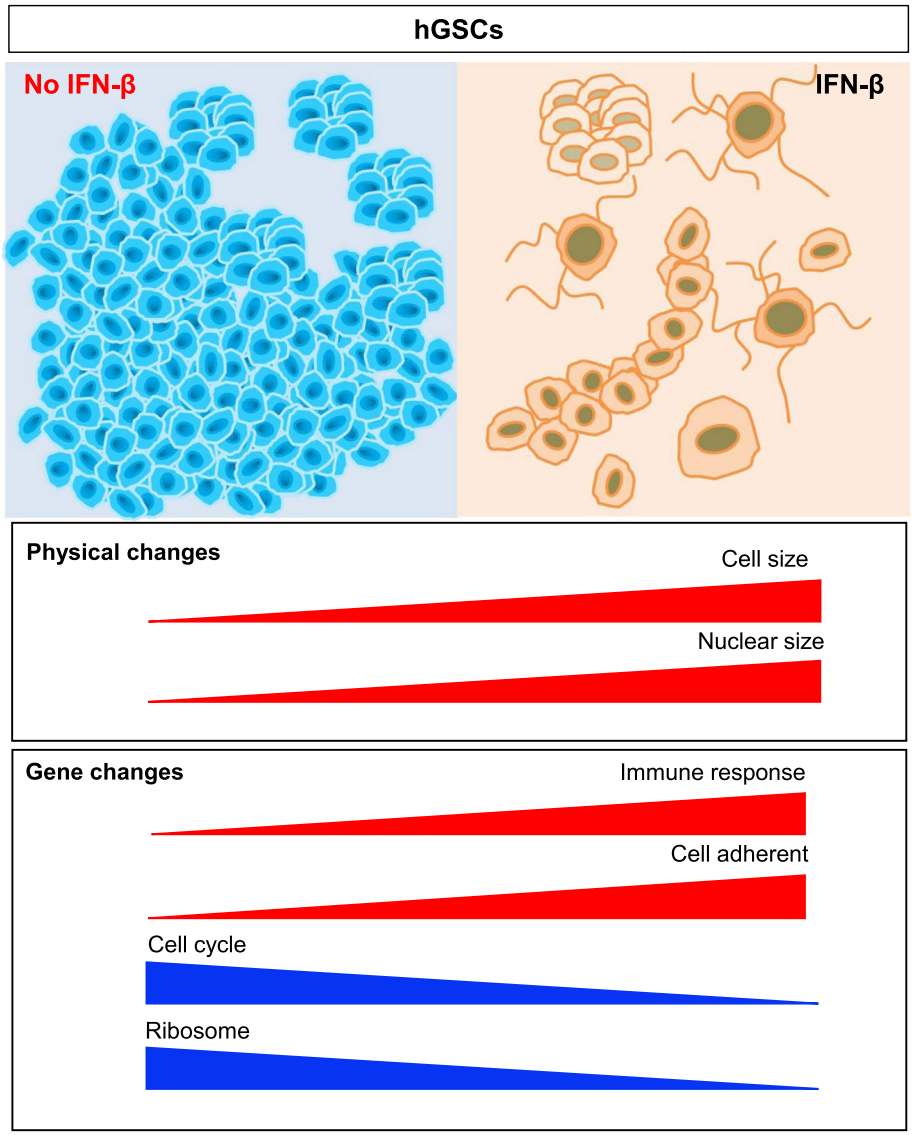

Fig. 6 IFN-β reduced cell proliferation in hGCSs. The ability to form spheres was inhibited by IFN-β. The cell and nuclear sizes of hGCSs increased after IFN-β treatment. On a gene level, significant upregulation was observed among immune response and cell adherence-related genes. Cell cycle and ribosome-related genes decreased

we washed the dishes with 1× phosphate-buffered saline (PBS). 5 μg/mL laminin was finally added to the dishes for at least 16 h. The coated dishes were stored at −20 °C for future use, and the supernatant was discarded before use.

Cell immunofluorescent staining

hGSCs were assessed using a staining assay, similar to that described in our previous study (Han et al. 2017). Briefly, hGSCs were cultured for 3 or 7 days in optimized culture conditions. Then, we fixed them in 4% paraformaldehyde (PFA) for 12 minutes. After cell fixation, 2.5% Triton X-100 in PBS were used to permeabilize cells with 15 minutes incubation. The supernatant was discarded for 1.5 hours cell blocking with 5% bovine serum albumin (Solarbio) in 1× PBS. All procedures were performed at room temperature. Primary antibodies including Sox2 (Goat, R&D), S100-β (Mouse, Abcam), or Ki67 (Rabbit, Thermo Fisher) were diluted as manufacturer protocol and added for 2 days incubation at 4 °C. Three times of wash were performed with 0.1% Tween-20 (Sigma) in 1× PBS. Secondary antibodies (Jackson Immuno Research), including Alexa Fluor 633-conjugated donkey anti-goat IgG antibody, Alexa Fluor 488-conjugated donkey anti-mouse IgG

antibody, Alexa Fluor Cy3-conjugated donkey anti-goat IgG antibody, and Alexa Fluor 633-conjugated donkey anti-rabbit antibody were dissolved in PBS containing 2.5% bovine serum albumin. After 2 hours incubation at room temperature, three times of wash were performed with 0.1% Tween-20 (Sigma) in 1× PBS again. Finally, 4′, 6-diamidino-2-phenylindole (DAPI, Sigma) diluted with 0.1% Tween-20 in PBS was used to stain the nuclei. An inverted fluorescence microscope (Nikon TE2000) was used to obtain images of the immunofluorescent-stained cells.

Sequencing and genomic analysis

We collected both hGSCs and hNSCs after 7 days of culture. After discarding the supernatant medium, 1× PBS was used to wash the cells once, and 2 ml Trizol (Invitrogen, Carlsbad, CA, USA) was added to each plate for RNA extraction. Agilent 2100 Bioanalyzer (Agilent, Palo Alto, CA, USA) was used to detect RNA integrity. Nanodrop (Thermo Fisher Scientific, Wilmington, DE, USA) was used to determine RNA quantity. Illumina TruSeqTM RNA sample preparation kit (Illumina Inc., San Diego, CA, USA) was used for fragmentation and cDNA synthesis priming. After that, ploy-T oligo-attached magnetic beads were used to purify poly-A containing mRNA molecules. All procedures were performed according to the manufacturer protocol. The cDNA was further converted into double-stranded DNA using the reagents supplied in the kit. AMpure XP beads were used to purify dsDNA. End-repaired and A-tailed were done according to Illumina's protocol. PCR was applied to enrich the DNA fragments with adapter molecules on both ends and to amplify the amount of DNA in the library after adapter ligation. We pooled together the resulting molecular libraries and sequenced on a HiSeq 2500 sequencer (Illumina Inc.). According to the gene expression base, the fragments per kilobase of transcript per million mapped reads (FPKM) values were analyzed. Online software (Morpheus, https://software.broadinstitute.org/morpheus) was used to perform Differentially expressed gene (DEG) analysis. Online database (g:Profiler) (Reimand et al. 2007) was used for Kyoto Encyclopedia of Genes and Genomes (KEGG) and Gene Ontology (GO) analyses.

Statistical analysis

All data were collected and analyzed based on three or more replicates. The error bars represent the standard deviation of the mean. Statistical analysis was performed using GraphPad Prism version 8.0.0 for Windows, GraphPad Software, San Diego, California USA, www.graphpad.comGraphPad Prism 7.0. For multiple comparisons, Student's t-test was used to determine significant differences. Significance is indicated as $^{*}p < 0.05$. $^{**}p < 0.01$, and $^{***}p < 0.001$.

Abbreviations

NSCs: Neural stem cells; GSCs: Glioma stem cells; IFN-β: Interferon-beta; hNSCs: Human NSCs; hGSCs: Human GSCs; CCNA2: Cyclin A2; CCNB1: Cyclin B1; CCNB2: Cyclin B1; CCND1: Cyclin D1; TME: Tumor microenvironment; JAK: Janus kinase–signal transducer; HBSS: Hank's Balanced Salt Solution; DMEM: Dulbecco's Modified Eagle Medium; MEF: Mouse embryonic fibroblast; TGF-β: Transforming growth factor-beta; PBS: Phosphate-buffered saline; PFA: Paraformaldehyde; FPKM: Fragments per kilobase of transcript per million mapped reads; DEG: Differentially expressed gene; KEGG: Kyoto Encyclopedia of Genes and Genomes; GO: Gene Ontology; BP: Biological process; CDK: Cyclin-dependent kinase; CD: Cytosine deaminase; 5-FC: 5-fluorocytosine.

Acknowledgments

We acknowledge all the lab members who provided assistance in this study.

Authors' contributions

CCH, HXX, and HH conceived and designed the research. HXX and JSK performed the sample collection, experiments, and data analysis. YLM, WM, HXY, HDY, and RJ assisted with the performance of cell-based experiments. ZMH, HW, and DJJ assisted with data analysis. CCH, HXX, and JSK wrote the manuscript. All authors have read and approved the final version of the manuscript.

Funding

This work was supported by funds from the National Natural Science Foundation of China [31600819 to CCH, 81901031 to HXX, 32070862 and 31571058 to GZL], the Shanghai Municipal Population and Family Planning Commission [20174Y0216 to CCH], the Natural Science Foundation of Shanghai [19ZR1445400 to HXX], the National Key R&D Program of China [2019YFA0110300], and the Shanghai Easter Scholar [8101219003 to GZL].

Availability of data and materials

The datasets used and/or analyzed during the current study are available from the corresponding author on reasonable request.

Declarations

Ethics approval and consent to participate

All human samples collection were carried out in accordance with Declaration of Helsinki, as well as under the guidance of Chinese National Guidelines GB/T 40352.1–2021 and GB/T 38736–2020. The patients/participants provided their written informed consent to participate in this study according to the permission from Ethics Committee of Shanghai 10th people's Hospital. All the human tissues were collected following clinical SOP under the patient's consent.

Consent for publication

Not applicable.

Competing interests

The authors declare that they have no competing interests.

Author details

[1]Shanghai Key Laboratory of Craniomaxillofacial Development and Diseases, Shanghai Stomatological Hospital & School of Stomatology, Fudan University, Shanghai, China. [2]Institute of Photomedicine, Shanghai Skin Disease Hospital, Tongji University School of Medicine, Shanghai, China. [3]School of Medicine, Jiaxing University, Jiaxing, China. [4]Tongji University Cancer Center, Shanghai Tenth People's Hospital, School of Medicine, Tongji University, Shanghai, China. [5]Department of Neurosurgery, Changzheng Hospital, Second Military Medical University, Shanghai, China. [6]Department of Neurosurgery, Third Affiliated Hospital of Second Military Medical University, Shanghai, China.

Received: 9 December 2021 Accepted: 6 May 2022
Published online: 02 July 2022

References

Abels ER, Broekman MLD, Breakefield XO, Maas SLN. Glioma EVs contribute to immune privilege in the brain. Trends Cancer. 2019;5:393–6.

Alcantara Llaguno S, Sun D, Pedraza AM, Vera E, Wang Z, Burns DK, et al. Cell-of-origin susceptibility to glioblastoma formation declines with neural lineage restriction. Nat Neurosci. 2019;22:545–55.

Bao S, Wu Q, McLendon RE, Hao Y, Shi Q, Hjelmeland AB, et al. Glioma stem cells promote radioresistance by preferential activation of the DNA damage response. Nature. 2006;444:756–60.

Borden EC, Lindner D, Dreicer R, Hussein M, Peereboom D. Second-generation interferons for cancer: clinical targets. Semin Cancer Biol. 2000;10:125–44.

Broekman ML, Maas SLN, Abels ER, Mempel TR, Krichevsky AM, Breakefield XO. Multidimensional communication in the microenvirons of glioblastoma. Nat Rev Neurol. 2018;14:482–95.

Cadart C, Monnier S, Grilli J, Saez PJ, Srivastava N, Attia R, et al. Size control in mammalian cells involves modulation of both growth rate and cell cycle duration. Nat Commun. 2018;9:3275.

Cantwell H, Nurse P. Unravelling nuclear size control. Curr Genet. 2019;65:1281–5.

Castets F, Griffin WS, Marks A, Van Eldik LJ. Transcriptional regulation of the human S100 beta gene. Brain Res Mol Brain Res. 1997;46:208–16.

Chen J, Li Y, Yu TS, McKay RM, Burns DK, Kernie SG, et al. A restricted cell population propagates glioblastoma growth after chemotherapy. Nature. 2012;488:522–6.

Chien AC, Hill NS, Levin PA. Cell size control in bacteria. Curr Biol. 2012;22:R340–9.

Corradetti B, Lange-Consiglio A, Barucca M, Cremonesi F, Bizzaro D. Size-sieved subpopulations of mesenchymal stem cells from intervascular and perivascular equine umbilical cord matrix. Cell Prolif. 2011;44:330–42.

Davis ME. Glioblastoma: overview of disease and treatment. Clin J Oncol Nurs. 2016;20:S2–8.

Dickson PV, Hamner JB, Burger RA, Garcia E, Ouma AA, Kim SU, et al. Intravascular administration of tumor tropic neural progenitor cells permits targeted delivery of interferon-beta and restricts tumor growth in a murine model of disseminated neuroblastoma. J Pediatr Surg. 2007;42:48–53.

Galli R, Binda E, Orfanelli U, Cipelletti B, Gritti A, De Vitis S, et al. Isolation and characterization of tumorigenic, stem-like neural precursors from human glioblastoma. Cancer Res. 2004;64:7011–21.

Garrison JI, Berens ME, Shapiro JR, Treasurywala S, FloydSmith G. Interferon-beta inhibits proliferation and progression through S phase of the cell cycle in five glioma cell lines. J Neuro-Oncol. 1996;30:213–23.

Han X, Yu L, Ren J, Wang M, Liu Z, Hu X, et al. Efficient and fast differentiation of human neural stem cells from human embryonic stem cells for cell therapy. Stem Cells Int. 2017;2017:9405204.

Han XX, Cai C, Yu LM, Wang M, Hu DY, Ren J, et al. A fast and efficient approach to obtaining high-purity glioma stem cell culture. Front Genet. 2021;12:639858.

Happold C, Roth P, Silginer M, Florea AM, Lamszus K, Frei K, et al. Interferon-beta induces loss of Spherogenicity and overcomes therapy resistance of glioblastoma stem cells. Mol Cancer Ther. 2014;13:948–61.

Hemmati HD, Nakano I, Lazareff JA, Masterman-Smith M, Geschwind DH, Bronner-Fraser M, et al. Cancerous stem cells can arise from pediatric brain tumors. P Natl Acad Sci USA. 2003;100:15178–83.

Herrmann A, Lahtz C, Song J, Aftabizadeh M, Cherryholmes GA, Xin H, et al. Integrin α6 signaling induces STAT3-TET3-mediated hydroxymethylation of genes critical for maintenance of glioma stem cells. Oncogene. 2020;39:2156–69.

Hu B, Wang Q, Wang YA, Hua S, Sauvé CG, Ong D, et al. Epigenetic activation of WNT5A drives glioblastoma stem cell differentiation and invasive growth. Cell. 2016;167:1281–1295.e1218.

Huang H, Yu X, Han X, Hao J, Zhao J, Bebek G, et al. Piwil1 regulates glioma stem cell maintenance and glioblastoma progression. Cell Rep. 2021;34:108522.

Ignatova TN, Kukekov VG, Laywell ED, Suslov ON, Vrionis FD, Steindler DA. Human cortical glial tumors contain neural stem-like cells expressing astroglial and neuronal markers in vitro. Glia. 2002;39:193–206.

Imbalzano E, Quartuccio S, Casciaro M, Gangemi S. S100B in heart diseases. Cardiovasc Pathol. 2020;49:107235.

Ito S, Natsume A, Shimato S, Ohno M, Kato T, Chansakul P, et al. Human neural stem cells transduced with IFN-beta and cytosine deaminase genes intensify bystander effect in experimental glioma. Cancer Gene Ther. 2010;17:299–306.

Jorgensen P, Edgington NP, Schneider BL, Rupes I, Tyers M, Futcher B. The size of the nucleus increases as yeast cells grow. Mol Biol Cell. 2007;18:3523–32.

Katsube Y, Hirose M, Nakamura C, Ohgushi H. Correlation between proliferative activity and cellular thickness of human mesenchymal stem cells. Biochem Biophys Res Commun. 2008;368:256–60.

Kendall SE, Najbauer J, Johnston HF, Metz MZ, Li S, Bowers M, et al. Neural stem cell targeting of glioma is dependent on phosphoinositide 3-kinase signaling. Stem Cells. 2008;26:1575–86.

Khsheibun R, Paperna T, Volkowich A, Lejbkowicz I, Avidan N, Miller A. Gene expression profiling of the response to interferon beta in Epstein-Barr-transformed and primary B cells of patients with multiple sclerosis. PLoS One. 2014;9:e102331.

Kim JY, Kim HJ, Jung CW, Choi BI, Lee DH, Park MJ. PARK7 maintains the stemness of glioblastoma stem cells by stabilizing epidermal growth factor receptor variant III. Oncogene. 2021;40:508–21.

Kim SK, Kim SU, Park IH, Bang JH, Aboody KS, Wang KC, et al. Human neural stem cells target experimental intracranial medulloblastoma and deliver a therapeutic gene leading to tumor regression. Clin Cancer Res. 2006;12:5550–6.

Le Rhun E, von Achenbach C, Lohmann B, Silginer M, Schneider H, Meetze K, et al. Profound, durable and MGMT-independent sensitivity of glioblastoma cells to cyclin-dependent kinase inhibition. Int J Cancer. 2019;145:242–53.

Li Q, Rycaj K, Chen X, Tang DG. Cancer stem cells and cell size: a causal link? Semin Cancer Biol. 2015;35:191–9.

Lohmann B, Le Rhun E, Silginer M, Epskamp M, Weller M. Interferon-beta sensitizes human glioblastoma cells to the cyclin-dependent kinase inhibitor, TG02. Oncol Lett. 2020;19:2649–56.

Mizuno M, Yoshida J. Effect of human interferon beta gene transfer upon human glioma, transplanted into nude mouse brain, involves induced natural killer cells. Cancer Immunol Immun. 1998;47:227–32.

Natsume A, Mizuno M, Ryuke Y, Yoshida J. Antitumor effect and cellular immunity activation by murine interferon-beta gene transfer against intracerebral glioma in mouse. Gene Ther. 1999;6:1626–33.

Natsume A, Tsujimura K, Mizuno M, Takahashi T, Yoshida J. IFN-beta gene therapy induces systemic antitumor immunity against malignant glioma. J Neuro-Oncol. 2000;47:117–24.

Neumann FR, Nurse P. Nuclear size control in fission yeast. J Cell Biol. 2007;179:593–600.

Ohtsuka T, Nakanishi H, Ikeda W, Satoh A, Momose Y, Nishioka H, et al. Nexilin: a novel actin filament-binding protein localized at cell-matrix adherens junction. J Cell Biol. 1998;143:1227–38.

Ostrom QT, Gittleman H, Xu J, Kromer C, Wolinsky Y, Kruchko C, et al. CBTRUS statistical report: primary brain and other central nervous system tumors diagnosed in the United States in 2009-2013. Neuro-Oncology. 2016;18:v1–v75.

Pfeffer LM, Kim JG, Pfeffer SR, Carrigan DJ, Baker DP, Wei L, et al. Role of nuclear factor-kappaB in the antiviral action of interferon and interferon-regulated gene expression. J Biol Chem. 2004;279:31304–11.

Platanias LC. Mechanisms of type-I- and type-II-interferon-mediated signalling. Nat Rev Immunol. 2005;5:375–86.

Reimand J, Kull M, Peterson H, Hansen J, Vilo J. g:Profiler--a web-based toolset for functional profiling of gene lists from large-scale experiments. Nucleic Acids Res. 2007;35:W193–200.

Schmidt NO, Przylecki W, Yang W, Ziu M, Teng Y, Kim SU, et al. Brain tumor tropism of transplanted human neural stem cells is induced by vascular endothelial growth factor. Neoplasia. 2005;7:623–9.

Shimato S, Natsume A, Takeuchi H, Wakabayashi T, Fujii M, Ito M, et al. Human neural stem cells target and deliver therapeutic gene to experimental leptomeningeal medulloblastoma. Gene Ther. 2007;14:1132–42.

Sims TL, Hamner JB, Bush RA, Williams RF, Zhou JF, Kim SU, et al. Neural progenitor cell-mediated delivery of interferon Beta improves neuroblastoma response to cyclophosphamide. Ann Surg Oncol. 2008;15:3259–67.

Son S, Tzur A, Weng Y, Jorgensen P, Kim J, Kirschner MW, et al. Direct observation of mammalian cell growth and size regulation. Nat Methods. 2012;9:910–2.
Stupp R, Mason WP, van den Bent MJ, Weller M, Fisher B, Taphoorn MJ, et al. Radiotherapy plus concomitant and adjuvant temozolomide for glioblastoma. N Engl J Med. 2005;352:987–96.
Su YT, Chen R, Wang H, Song H, Zhang Q, Chen LY, et al. Novel targeting of transcription and metabolism in glioblastoma. Clin Cancer Res. 2018;24:1124–37.
Taga T, Tabu K. Glioma progression and recurrence involving maintenance and expansion strategies of glioma stem cells by organizing self-advantageous niche microenvironments. Inflamm Regen. 2020;40:33.
Tang Y, Yu P, Cheng L. Current progress in the derivation and therapeutic application of neural stem cells. Cell Death Dis. 2017;8:e3108.
Tian A, Kang B, Li B, Qiu B, Jiang W, Shao F, et al. Oncogenic state and cell identity Combinatorially dictate the susceptibility of cells within glioma development hierarchy to IGF1R targeting. Adv Sci (Weinh). 2020;7:2001724.
Turner JJ, Ewald JC, Skotheim JM. Cell size control in yeast. Curr Biol. 2012;22:R350–9.
Venkatesh HS, Johung TB, Caretti V, Noll A, Tang Y, Nagaraja S, et al. Neuronal activity promotes glioma growth through Neuroligin-3 secretion. Cell. 2015;161:803–16.
Wang X, Zhou R, Xiong Y, Zhou L, Yan X, Wang M, et al. Sequential fate-switches in stem-like cells drive the tumorigenic trajectory from human neural stem cells to malignant glioma. Cell Res. 2021;31(6):684–702.
Wu J, Bryla C, Mccoy A, Lisa B, Garren N, Siegel C, et al. Phase I trial of Tg02 plus dose-dense or metronomic Temozolomide for adults with recurrent anaplastic astrocytoma and glioblastoma. Neuro-Oncology. 2017;19:15.
Yagi K, Hayashi Y, Ishida N, Ohbayashi M, Ohishi N, Mizuno M, et al. Interferon-Beta endogenously produced by Intratumoral injection of cationic liposome-encapsulated gene - Cytocidal effect on glioma transplanted into nude-mouse brain. Biochem Mol Biol Int. 1994;32:167–71.
Yamamuro S, Sano E, Okamoto Y, Ochiai Y, Ohta T, Ogino A, et al. Antitumorigenic effect of interferon-beta by inhibition of undifferentiated glioblastoma cells. Int J Oncol. 2015;47:1647–54.
Yamazoe T, Koizumi S, Yamasaki T, Amano S, Tokuyama T, Namba H. Potent tumor tropism of induced pluripotent stem cells and induced pluripotent stem cell-derived neural stem cells in the mouse intracerebral glioma model. Int J Oncol. 2015;46:147–52.
Yang CH, Murti A, Pfeffer SR, Basu L, Kim JG, Pfeffer LM. IFNalpha/beta promotes cell survival by activating NF-kappa B. Proc Natl Acad Sci U S A. 2000;97:13631–6.

Publisher's Note